International Journal of Engineering Science 169 (2021) 103577

Contents lists available at ScienceDirect

International Journal of Engineering Science

journal homepage: www.elsevier.com/locate/ijengsci

On the evaluation of non-Fourier effects in heat pulse experiments

A. Fehér [a], R. Kovács [a,b,c,*]

[a] Department of Energy Engineering, Faculty of Mechanical Engineering, BME, Budapest, Hungary
[b] Department of Theoretical Physics, Wigner Research Centre for Physics, Institute for Particle and Nuclear Physics, Budapest, Hungary
[c] Montavid Thermodynamic Research Group, Hungary

ARTICLE INFO

Keywords:
Flash experiments
Non-Fourier heat conduction
Analytical solutions

ABSTRACT

The heat pulse (flash) experiment is a well-known and widely accepted method to measure the thermal diffusivity of a material. In recent years, it has been observed that the thermal behavior of heterogeneous materials can show deviation from the classical Fourier equation, resulting in a different thermal diffusivity and requiring further thermal parameters to identify. Such heterogeneity can be inclusions in metal foams, layered structure in composites, or even cracks and porous parts in rocks. Furthermore, the next candidate, the Guyer–Krumhansl equation is tested on these experiments with success. However, these recent evaluations required a computationally intensive fitting procedure using countless numerical solutions, even when a good initial guess for the parameters is found by hand. This paper presents a Galerkin-type discretization for the Guyer–Krumhansl equation, which helped us find a reasonably simple analytical solution for time-dependent boundary conditions. Utilizing this analytical solution, we developed a new evaluation technique to immediately estimate all the necessary thermal parameters using the measured temperature history.

1. Introduction

Engineering requires reliable ways to determine the parameters necessary to characterize the behavior of materials. In what follows, we place our focus on the thermal description of materials, especially on heterogeneous materials such as rocks and foams. Although there is a so-called representative size for such materials for which the local spatial variations vanish, this is not necessarily a practically realizable property. In other words, either the commercial measurement device or the practical application might not allow a sample with such size to be used. Consequently, there is a need to investigate the thermal behavior of materials in which heterogeneities play a role and that might therefore require additional parameters to characterize. In recent papers Both et al. (2016) and Ván et al. (2017), it is reported that the presence of various heterogeneities can result in a non-Fourier heat conduction effect on the macro-scale under room temperature conditions due to the simultaneous presence of heat conduction channels with different characteristic times. A particular case is depicted in Fig. 1 for a capacitor sample with a periodic layered structure in which a good conductor and an insulator alternately follow each other. Such effects are observed in a flash (or heat pulse) experiment in which the front side of the specimen is excited with a short heat pulse and the temperature is measured at the rear side (James, 1980; Parker, Jenkins, Butler, & Abbott, 1961). That temperature history is used to find the thermal diffusivity in order to characterize the transient material behavior. On the front side, a very thin graphite layer is situated to ensure the maximum absorption of the heat pulse. Therefore, the heat source can be modeled with proper boundary conditions instead of a spatial-dependent transient volumetric heat source.

* Corresponding author at: Department of Theoretical Physics, Wigner Research Centre for Physics, Institute for Particle and Nuclear Physics, Budapest, Hungary.
E-mail address: kovacs.robert@wigner.hu (R. Kovács).

https://doi.org/10.1016/j.ijengsci.2021.103577
Received 25 May 2021; Received in revised form 24 August 2021; Accepted 26 August 2021

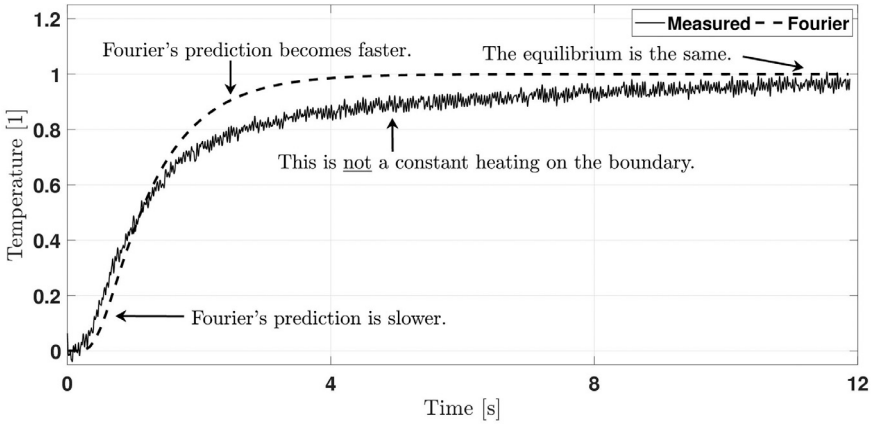

Fig. 1. Measured rear side temperature history for the capacitor sample and the prediction provided by Fourier's theory (Both et al., 2016).

The non-Fourier effect occurs on a specific time interval, as Fig. 1 shows for a typical outcome of the flash experiments; this is called over-diffusion. After that interval, the Fourier equation appears to be a suitable choice for modeling, as the influence of the heterogeneities vanishes (later we show further examples). Also, there is no difference between the steady-states described by the Fourier and non-Fourier heat equations; merely the transient evolution of temperature differs in these cases. Based on our experimental experience, the occurrence of over-diffusion depends on various factors, for instance, sample thickness, characteristic parallel time scales, and excitation (i.e., boundary conditions) (Fülöp et al., 2018).

The evaluation procedure of flash experiments with non-Fourier heat equations is not yet standardized. Finding the solution of non-Fourier models even numerically is not straightforward, and certain methods can lead to false solutions, too (Rieth, Kovács, & Fülöp, 2018); moreover, the commercial, built-in algorithms are not efficient for these models. The present paper aims to develop a reliable and resource-friendly way for the fitting procedure, analogous to how the Fourier equation is applied for flash experiments.

In the following sections, we organize the discussion as follows. First, we briefly introduce the two heat conduction models for the heat pulse experiments and evaluations with a particular set of dimensionless quantities. Second, we shortly present how a complete evaluation with the Fourier heat equation can be conducted. Then, we carry out the evaluation procedure with the Guyer–Krumhansl equation. After that, we demonstrate the benefits of this fitting procedure and revisit some previous measurements. Furthermore, we decided to place the derivation of the analytical solutions to the end of the paper as an Appendix. To the best of our knowledge, the Galerkin method has not been used before for the Guyer–Krumhansl equation and this is a novel result in this respect. Here, the focus on its practical utilization.

2. Models for heat pulse experiments

Although numerous generalizations of Fourier's law exist in the literature (Cimmelli, 2009; Joseph & Preziosi, 1989; Müller & Ruggeri, 1998; Sobolev, 1997, 2014; Ván, 2016), there is only one of them that has indeed proved to be reasonable as the next candidate beyond Fourier's theory, the Guyer–Krumhansl (GK) equation. This constitutive equation reads in one spatial dimension

$$\tau_q \partial_t q + q + \lambda \partial_x T - \kappa^2 \partial_{xx} q = 0. \tag{1}$$

Here, τ_q is the relaxation time for the heat flux q and κ^2 is a kind of 'dissipation parameter', usually related to the mean free path in kinetic theory. Whereas it was first derived on the basis of kinetic theory (Guyer & Krumhansl, 1966a), this model also has a strong background in non-equilibrium thermodynamics with internal variables (NET-IV) (Ván, 2001; Ván & Fülöp, 2012). While in kinetic theory an underlying mechanism for phonons is assumed, this is entirely neglected in the case of NET-IV, leaving the coefficients to be free (however, their sign is restricted by the second law of thermodynamics). Eq. (1) is a time evolution equation for the heat flux, and in order to have a mathematically and physically complete system, we need the balance of internal energy e, too,

$$\rho c \partial_t T + \partial_x q = 0, \tag{2}$$

in which the equation of state $e = cT$ is used with c being the specific heat and ρ is the mass density. All these coefficients are constant, only rigid bodies are assumed with no volumetric heat source.

At this point, we owe an explanation of why we do not deal with the Maxwell–Cattaneo–Vernotte (MCV) equation.

(1) Hyperbolicity vs. parabolicity. It is usually claimed that a heat equation model should be hyperbolic, as is the MCV theory, describing finite propagation speed. Indeed, this seems reasonable, but it does not help in practical application under common conditions (room temperature, heterogeneous materials). The Fourier equation is still well-applicable in spite of its parabolic nature, therefore we do not see it as a decisive property.

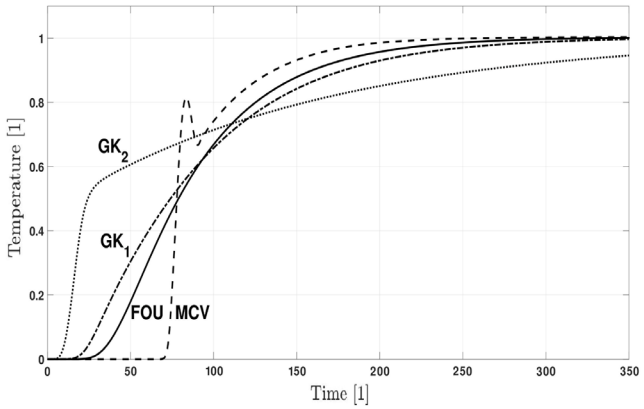

Fig. 2. Typical rear side temperature histories for the Fourier ('FOU'), Maxwell–Cattaneo–Vernotte (MCV), and Guyer–Krumhansl ('GK1' and 'GK2') equations. For the GK model, two different solutions are depicted: 'GK1' is slightly over-diffusive and shows similar outcomes to the experiments, while 'GK2' is a strongly over-diffusive solution.

(2) In a low-temperature situation, the MCV model was sound, primarily due to the observed wave phenomenon in super-fluids, called second sound (Landau, 1947; Tisza, 1938). The GK equation, despite its parabolic nature, also helped researchers find the second sound in solids as well (Guyer & Krumhansl, 1966b).
(3) There has been significant effort put into searching for the trace of wave propagation at room temperature (in a macro-scale object, so nano-structures does not count now), sadly with no success (Józsa & Kovács, 2020; Mitra, Kumar, Vedevarz, & Moallemi, 1995).
(4) Fig. 2 shows the typical rear side temperature responses for the Fourier, MCV and GK models. Apparently, while the MCV equation adds a sharp wavefront to the solution, the GK equation provides a significantly better match with the measured data. Therefore the GK equation appears to be the minimal necessary extension of the Fourier equation, which covers the needs of engineering practice.
(5) There are higher-order models as well, such as ballistic-diffusive models (Dreyer & Struchtrup, 1993; Kovács & Ván, 2015; Müller & Ruggeri, 1998), but they are related to a different research program, and for this work, investigating macro-scale objects, they do not seem relevant.
(6) On the analogy of the MCV model, the so-called dual-phase lag (DPL) equation (Tzou, 2014) is often used as the best candidate after Fourier's law. Sadly, this model introduces two time constants in an ad hoc manner, violating basic physical principles (Rukolaine, 2014, 2017), leading to mathematically ill-posed problems as well (Fabrizio & Franchi, 2014; Fabrizio, Lazzari, & Tibullo, 2017). In contrast, the GK equation has a strict thermodynamic background in which the new coefficients originate from the Onsagerian relations and are restricted by the second law (Ván & Fülöp, 2012). Moreover, since the derivation of the GK equation exploits the energy balance (2) as a constraint, (2) is naturally satisfied. This has not been investigated for the DPL model.

Last but not least, we also must mention a relatively little-known model from the literature, the Nyíri equation (Nyíri, 1991),

$$q + \lambda \partial_x T - \kappa^2 \partial_{xx} q = 0, \tag{3}$$

which is similar to the Guyer–Krumhansl model but leaves the time lagging effects out of sight, hence it is purely a spatially nonlocal heat equation. Testing its solutions with the method presented in the Appendix turned out to be inaccurate for measurements, unfortunately. Consequently, the GK model is indeed the simplest but necessary extension for the Fourier equation, as neither the MCV nor the Nyíri model is capable of describing these experiments accurately. In other words, the two new parameters (τ_q and κ^2) are truly needed for our analysis. Apparently, there are numerous available models in the literature, and it is important to carefully consider the characteristic spatial and time scales and choose the model accordingly.

2.1. *T* and *q*-representations

Depending on the purpose, it is useful to keep in mind that for such linear models, it is possible to chose a 'primary' field variable, which could ease the definition of the boundary conditions in some cases. For the GK equation, the temperature T and the heat flux q are the candidates, and their forms are

$$\text{T-representation:} \quad \tau_q \partial_{tt} T + \partial_t T - \alpha \partial_{xx} T - \kappa^2 \partial_{txx} T = 0, \tag{4}$$

$$\text{q-representation:} \quad \tau_q \partial_{tt} q + \partial_t q - \alpha \partial_{xx} q - \kappa^2 \partial_{txx} q = 0. \tag{5}$$

We note that in T-representation, it is unknown how to define the boundary condition for q since it requires knowledge of $\partial_{xx} q$. On the other hand, in q-representation, it becomes meaningless to speak about T-boundaries. In a previous analytical solution for the GK

equation (Kovács, 2018), this difference was inevitable to realize. In the present work, we use the system (1)–(2). It is also interesting to notice that the GK model can recover the solution of the Fourier equation when $\kappa^2/\tau_q = \alpha$, this is called Fourier resonance (Both et al., 2016; Fülöp, Kovács, & Ván, 2015). These coefficients represent the existence of parallel heat transfer channels, introducing two characteristic time scales into the model. There is also a remarkable similarity between Eq. (4) and the so-called two-temperature model of Sobolev (Sobolev, 1994, 2016). In this model, it is supposed that there are two heat conduction channels, both obeying the Fourier law, that are coupled through the balance equations. A similar T-representation can be obtained for the average temperature. Although its outcome is close to the GK equation, it is different and could be restricted to samples in which the constituents are known. Overall, in the GK equation, the coefficients τ_q, α, and κ^2 must be fitted to the given temperature history.

2.2. Dimensionless set of parameters

Following Both et al. (2016), we introduce these definitions for the dimensionless parameters (quantities with hat):

$$\begin{aligned}
&\text{time and spatial coordinates:} && \hat{t} = \frac{t}{t_p} \quad \text{and} \quad \hat{x} = \frac{x}{L};\\
&\text{thermal diffusivity:} && \hat{\alpha} = \frac{\alpha t_p}{L^2} \quad \text{with} \quad \alpha = \frac{\lambda}{\rho c};\\
&\text{temperature:} && \hat{T} = \frac{T - T_0}{T_{\text{end}} - T_0} \quad \text{with} \quad T_{\text{end}} = T_0 + \frac{\bar{q}_0 t_p}{\rho c L};\\
&\text{heat flux:} && \hat{q} = \frac{q}{\bar{q}_0} \quad \text{with} \quad \bar{q}_0 = \frac{1}{t_p}\int_0^{t_p} q_0(t)\mathrm{d}t;\\
&\text{heat transfer coefficient:} && \hat{h} = h\frac{t_p}{\rho c};
\end{aligned} \tag{6}$$

together with $\hat{\tau}_q = \frac{\tau_q}{t_p}$, $\hat{\kappa}^2 = \frac{\kappa^2}{L^2}$, where $\hat{t}$ differs from the usual Fourier number in order to decouple the thermal diffusivity from the time scale in the fitting procedure. Furthermore, t_p denotes the constant heat pulse duration for which interval $\bar{q}_0$ averages the heat transferred with the heat pulse defined by $q(x = 0, t) = q_0(t)$ on the boundary. Here, L is equal to the sample thickness. T_{end} represents the adiabatic steady-state, and T_0 is the uniform initial temperature. In the rest of the paper, we shall omit the hat notation, otherwise we add the unit for the corresponding quantity. Utilizing this set of definitions, we obtain the dimensionless GK model:

$$\begin{aligned}
\partial_t T + \partial_x q &= 0,\\
\tau_q \partial_t q + q + \alpha \partial_x T - \kappa^2 \partial_{xx} q &= 0.
\end{aligned} \tag{7}$$

The initial condition is zero for both fields. For further details, we refer to the Appendix in which we present the analytical solution for the two heat equations. Also, we leave the discussion of the boundary conditions to the Appendix as well since it is only a technical detail that is less relevant in regard to the evaluation procedure. This set of dimensionless parameters does not change the definition of the Fourier resonance condition, i.e., it remains $\hat{\kappa}^2/\hat{\tau}_q = \hat{\alpha}$.

3. Evaluation with the Fourier theory

The analytical solution of the Fourier equation is found for the rear side in the form of

$$T(x = 1, t) = Y_0 \exp(-ht) - Y_1 \exp(x_F t), \quad x_F = -2h - \alpha\pi^2, \quad t > 30, \tag{8}$$

which is analogous with the classically known 'one-term solution', i.e., Eq. (8) is only the first term of an infinite series, and after $t > 30$, it provides solution with enough precision (as further terms converge to zero much faster, see Fig. 12 for demonstrative solutions). Here, we refer to the Appendix regarding the precise derivation together with the boundary conditions and the coefficients. Let us place our focus on the practical application of such a solution. First, we must estimate the heat transfer coefficient h by choosing arbitrarily two temperature values (T_1 and T_2) in the decreasing part of the temperature history (see the green part in Fig. 3) and read the corresponding time instants (t_1 and t_2). In this region, $\exp(x_F t) \approx 0$, thus

$$h = -\frac{\ln(T_2/T_1)}{t_2 - t_1}. \tag{9}$$

Whereas h is determined only by the rear side temperature history, one must keep in mind that the sample is small, and as long as $h \cdot A_h$ is constant (A_h is the surface where heat transfer occurs), it is not required to define a set of heat transfer coefficients for all surfaces and therefore h remains eligible. For the Fourier theory, it is possible to express the thermal diffusivity explicitly, i.e.,

$$\alpha_F = 1.38\frac{L^2}{\pi^2 t_{1/2}}, \tag{10}$$

and after registering $t_{1/2}$, it can be directly determined. This is the ratio of the thermal conductivity λ and the specific heat capacity ρc. Then, the top of the temperature history ($T_{\max}$) follows by reading the time instant ($t_{\max}$) when $T_{\max}$ occurs. Fig. 3 schematically summarizes this procedure. Overall, we obtained the heat transfer coefficients, the thermal diffusivity, and $T_{\max}$, which are all used for the Guyer–Krumhansl theory.

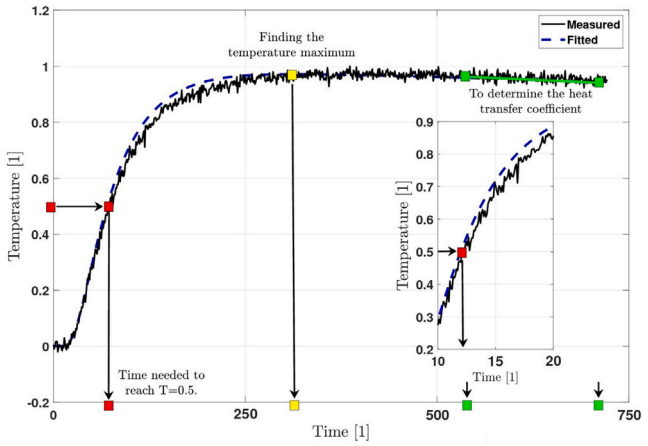

Fig. 3. Schematically presenting the evaluation method using Fourier's theory. The green part indicates the determination of the heat transfer coefficient, and the red squares show the meaning of $t_{1/2}$.

4. Evaluation with the Guyer–Krumhansl theory

The situation here becomes more difficult since this non-Fourier theory consists of two 'time constants' (x_1 and x_2) instead of one (x_F in the Fourier theory). Consequently, it is not possible to find these exponents without simplifications, in which one must be immensely careful. We prepared 'parameter maps' for all possible τ_q and κ^2 values that could be practically possible and beyond in order to check the effect of the simplifications made in the following. However, we still had to restrict ourselves to a domain, which is $3 > \kappa^2/(\alpha\tau_q) \geq 1$. Its lower limit expresses the Fourier case, and any other combination falls in the over-diffusive region. The highest experimentally observed ratio so far is around 2.5, thus we expect 3 to be eligible. For κ^2, we consider $0.02 < \kappa^2 < 1$. We want to emphasize that the GK theory itself is not restricted on to this domain; it would allow under-diffusive ('wave-like') propagation as well, which would be more similar to the MCV solution depicted in Fig. 2 (Guyer & Krumhansl, 1966b). However, for the present situation, we consider it beyond the range of this study due to the lack of experimental observations of room temperature experiments on macro-scale heterogeneous samples. In the GK theory, we can express the rear side temperature history as

$$T(x=1, t>40) = Y_0 \exp(-ht) - Z_1 \exp(x_1 t) - Z_2 \exp(x_2 t), \quad x_1, x_2 < 0, \tag{11}$$

which is also a 'one-term solution'; for the detailed calculation, parameter and boundary condition definitions, we again refer to the Appendix together with Fig. 13 in regard to convergence properties. This can be equivalently formulated realizing that $Z_2 = -P_0 - Z_1$,

$$T(x=1, t) = Y_0 \exp(-ht) - Z_1 \big(\exp(x_1 t) - \exp(x_2 t)\big) + P_0 \exp(x_2 t), \tag{12}$$

where merely one simplification becomes possible for all τ_q and κ^2: $\exp(x_1 t) \gg \exp(x_2 t)$ when $t > 60$, i.e.,

$$T(x=1, t>60) = Y_0 \exp(-ht) - Z_1 \exp(x_1 t) + P_0 \exp(x_2 t). \tag{13}$$

This form is more advantageous because P_0 remains practically constant for a given boundary condition and thus its value can be assumed a priori, which is exploited in the evaluation method. Now, let us present step by step the determination of GK parameters, depicted in Fig. 4.

- Step 1/A. We observe that the temperature predicted by Fourier's theory always coincides with the measured value at the beginning, after that, it rises faster at the top. In other words, in this region, the same temperature value (usually around 0.7–0.95) is reached sooner. Mathematically, we can express it by formally writing the equations for the Fourier and GK theories as follows:

$$T_F = Y_0 \exp(-ht) - Y_1 \exp(x_F t_F); \quad T_{GK} = Y_0 \exp(-ht_m) - Z_1 \exp(x_1 t_m) + P_0 \exp(x_2 t_m), \tag{14}$$

where the t_F time instant is smaller than the measured t_m, also $T_F = T_{GK}$ holds. Let us choose two such temperatures arbitrarily; taking their ratio, it yields

$$\exp\big(x_F(t_{F1} - t_{F2})\big) = \exp\big(x_1(t_{m1} - t_{m2})\big) \frac{-Z_1 + P_0 \exp\big((x_2 - x_1)t_{m1}\big)}{-Z_1 + P_0 \exp\big((x_2 - x_1)t_{m2}\big)}, \tag{15}$$

where the fraction on the right hand side is close to 1, mostly between 1 and 1.05 for 'small' time intervals. It could be possible to introduce it as a correction factor (denoted with c below) for x_1 in an iterative procedure if more to be known about τ_q

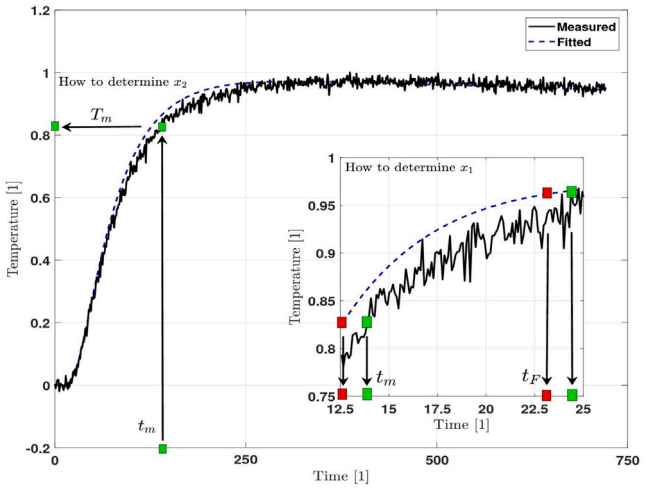

Fig. 4. The schematic representation of the evaluation method using the Guyer–Krumhansl theory. Here, the fitted curve belongs to the Fourier equation.

and κ^2. After rearrangement, we obtain a closed form formula for x_1:

$$x_1 = \frac{\ln(1/c)}{t_{m1} - t_{m2}} + x_F \frac{t_{F1} - t_{F2}}{t_{m1} - t_{m2}}. \tag{16}$$

Taking $c = 1$ is equivalent with neglecting $\exp(x_2 t)$ from the beginning around reaching $T_{\max}$, and leading to this same expression. Eventually, it introduces a correction for the Fourier exponent x_F based on the deviation from the measured data with the possibility to apply further corrections using c if needed. Practically, we take the 80% and 90% of $T_{\max}$ and for the next 20 subsequent measurement points, then we consider their mean value to be x_1. From a mathematical perspective, closer data point pairs should perform better, but this does not occur due to the uncertainty in the measurement data. In our experience, it offers a more consistent value for x_1.

- Step 1/B. In parallel with part A, we can determine the coefficient Z_1 for each t_m and for each corresponding $x_{1,m}$, that is,

$$Z_{1,m} = -\exp(-x_{1,m} t_m)\Big(T_m - Y_0 \exp(-h t_m)\Big) \tag{17}$$

where the subscript m denotes the value related to one measurement point. Also, after 20 subsequent points, we take the mean value of the set $\{Z_{1,m}\}$.

- Step 2. At this point, we can exploit that P_0 is 'almost constant', i.e., $2 < -P_0 < 2.03$ holds. Here, 2.03 comes from the parameter sweep; we did not observe higher values for $-P_0$, and also, it cannot be smaller than 2. This property allows us to a priori assume its value (such as $P_0 = -2.015$), and in a later step, we must fine-tune since the overall outcome reacts sensitively. Using P_0, we can obtain $Z_2 = -P_0 - Z_1$. In order to obtain x_2, we can rearrange the equation

$$T = Y_0 \exp(-ht) - Z_1 \exp(x_1 t) - Z_2 \exp(x_2 t) \tag{18}$$

for x_2, and calculate it as a mean value of the set $\{x_{2,m}\}$ filled with values related to each t_m. With noisy data, this approach can result in positive x_2 values, unfortunately. These values must be excluded, otherwise it leads to instability and a meaningless outcome. Careful data filtering can help to solve this shortcoming, and in fact, we used it to ease the calculation (the details are given in the next section).

- Step 3. Now, having both exponents and coefficients, it is possible to rearrange the analytical expressions to the GK parameters explicitly and calculate α_{GK}, τ_q and κ^2:

$$x_1, x_2 \Rightarrow k_1, k_2; \quad Z_1 \Rightarrow DP_0 \Rightarrow M_1, M_2 \Rightarrow \tau_q \Rightarrow \alpha_{GK} \Rightarrow \kappa^2. \tag{19}$$

For the detailed parameter definitions, we refer to Appendix.

- Step 4. As mentioned in Step 2, the overall outcome is sensitive to P_0. Therefore we choose to make a sweep on the possible interval with the step of 0.002, producing the temperature history for each set of parameters and characterizing them with R^2, the coefficient of determination. Lastly, we chose the best set.

Practically, this evaluation method reduces the number of 'fitted' parameters, as only P_0 has to be fine-tuned at the end. Besides, it is constrained into a relatively narrow range; consequently, the overall evaluation procedure takes only a few seconds to perform computationally intensive algorithms instead of hours.

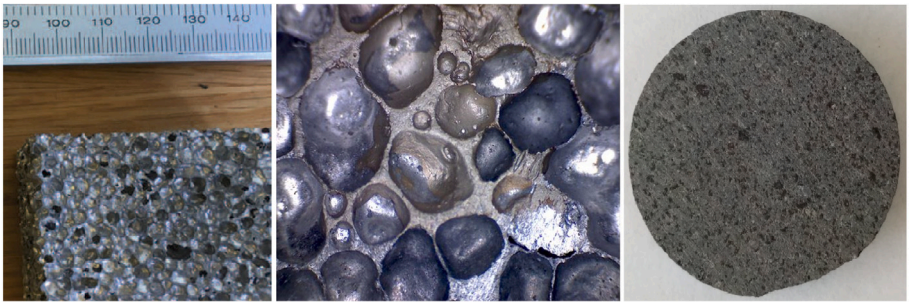

Fig. 5. Magnified view of the metal foam specimen (center) and the basalt rock sample (right).

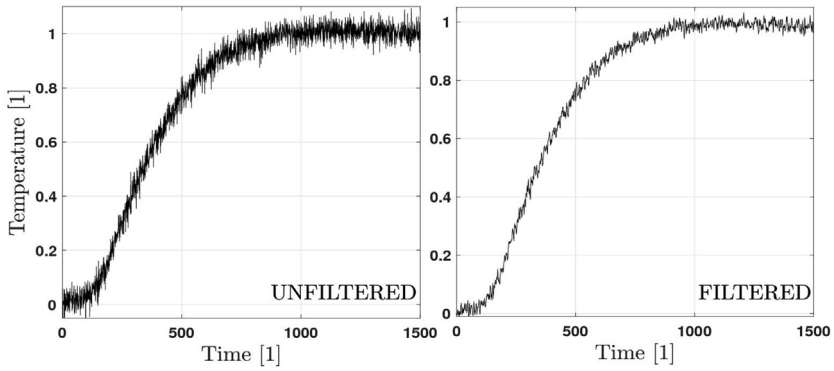

Fig. 6. The effect of data smoothing, using 10 neighboring points in the Savitzky–Golay algorithm.

5. Comparison with preceding experiments

First, we revisit the experiments presented in Fülöp et al. (2018), since that set of data on Basalt rock samples with thicknesses of 1.86, 2.75 and 3.84 mm, showed size dependence on both the thermal diffusivity and the non-Fourier effects. However, the fitted parameters in Fülöp et al. (2018) were found by hand, and are thus not exactly precise. Here, we aim to specify the exact quantities for the GK model and establish a more robust theoretical basis for the observations. Second, we reevaluate the data recorded on a metal foam sample with 5.2 mm thickness. This belongs among the samples showing the potent non-Fourier effect, presented first in Ván et al. (2017). Fig. 5 shows these samples.

Concerning heterogeneous materials, there is a representative size for which the effect of local heterogeneities vanishes; thus, one could obtain the global thermal properties of the sample. On the one hand, however, that size could be much larger than the limits for measurement devices. For instance, the present metal foam sample has inclusions in a millimeter scale, therefore its 5 mm thickness might not be representative, which would require samples that are three or four times larger. The usual thickness limit for a commercial laser flash device is around 6 mm, hence the representative size could be much larger than that. On the other hand, engineering applications might require the use of a heterogeneous material under its representative size, whose thermal behavior could differ from Fourier's law. Overall, there is a solid need to characterize such samples, too, and we aim to develop this procedure.

We note that samples are produced by ROCKSTUDY Ltd. and Admatis Ltd. (Hungary) since the required particular infrastructure and technology are all available there. For example, it is challenging to prepare a rock sample with 1.8 mm thickness due to its fragility; thus, we received only one sample from each. Therefore, we emphasize that the determination of precise thermal parameters would require more samples from the same size, but this falls beyond the limits of the present paper. For our aim – to develop and test the evaluation procedure – this is satisfactory.

In some cases, the available data is too noisy for such an evaluation method: an example is presented in Fig. 6. That data is smoothed using the built-in Savitzky–Golay algorithm of Matlab. We were careful not to overly smooth it in order to keep the physical content as untouched as possible.

5.1. Basalt rock samples

Regarding the exact details of measurements, we refer to Fülöp et al. (2018). Tables 1 and 2 consist of our findings using this evaluation algorithm. Comparing the outcomes of the two fitting procedures, we find the thermal diffusivities to be close to each other. However, this is not the case with the GK parameters τ_q and κ^2, which significantly differ from the previous values from Fülöp

Table 1
Summarizing the fitted thermal parameters.

Basalt rock samples	Findings in Fülöp et al. (2018)				Refined results			
	α_F 10^{-6} [m^2/s]	α_{GK} 10^{-6} [m^2/s]	τ_q [s]	κ^2 10^{-6} [m^2]	α_F 10^{-6} [m^2/s]	α_{GK} 10^{-6} [m^2/s]	τ_q [s]	κ^2 10^{-6} [m^2]
1.86 mm	0.62	0.55	0.738	0.509	0.68	0.61	0.211	0.168
2.75 mm	0.67	0.604	0.955	0.67	0.66	0.61	0.344	0.268
3.84 mm	0.685	0.68	0.664	0.48	0.70	0.68	1	0.65

Table 2
Characterizing the non-Fourier behavior using the Fourier resonance condition.

$\frac{\kappa^2}{\tau_q \alpha}$	Findings in Fülöp et al. (2018)	Refined values
1.86 mm	1.243	1.295
2.75 mm	1.171	1.272
3.84 mm	1.06	0.94

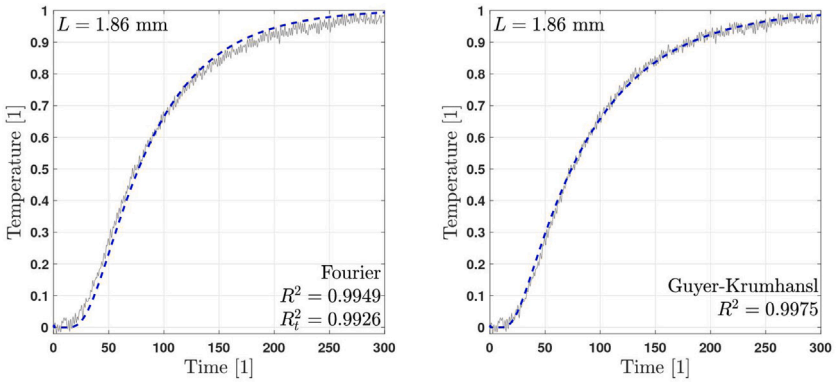

Fig. 7. The rear side temperature history for the basalt rock sample with $L = 1.86$ mm.

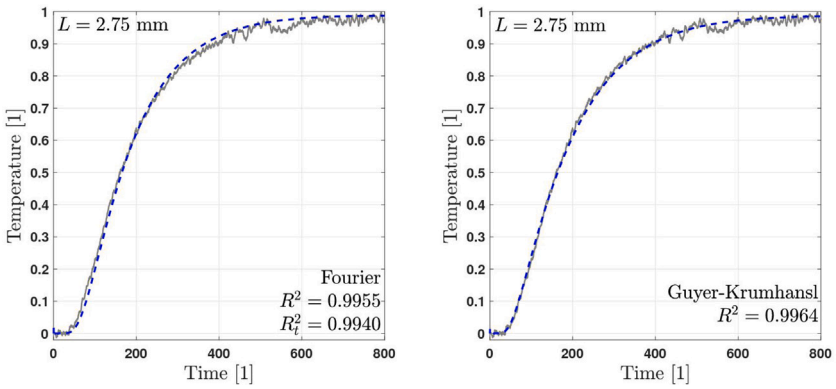

Fig. 8. The rear side temperature history for the basalt rock sample with $L = 2.75$ mm.

et al. (2018). Despite the huge difference, the size dependence for both the Fourier and non-Fourier behaviors is apparent. The fitted temperature histories are depicted in Figs. 7–10 for each thickness. Each figure shows the R^2 value for the fitted curve. For the Fourier solution, two curves are given: R_t^2 represents the data without any fine-tuned thermal diffusivity, this is purely theoretical. The other R^2 stands for the fine-tuned α_F.

In the first case ($L = 1.86$ mm), although the difference for the non-Fourier samples seems negligible, it results in a 10% difference in the thermal diffusivity. This is more visible from Table 2, in which the Fourier resonance condition spectacularly characterizes the deviation from Fourier's theory, decreasing for thicker samples. Regarding the third one ($L = 3.84$ mm), Fourier's theory seems to be 'perfectly splendid', and the GK model hardly improves it. Indeed, the 0.94 for the Fourier resonance is close enough to 1 to consider it to be a Fourier-like propagation.

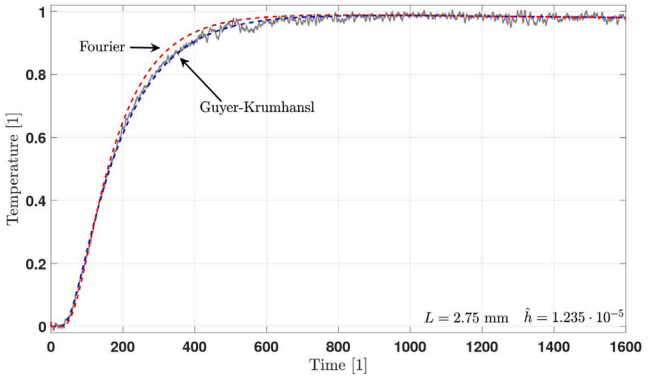

Fig. 9. Demonstrating the complete fitting for the rear side temperature in case of the basalt rock sample with $L = 2.75$ mm.

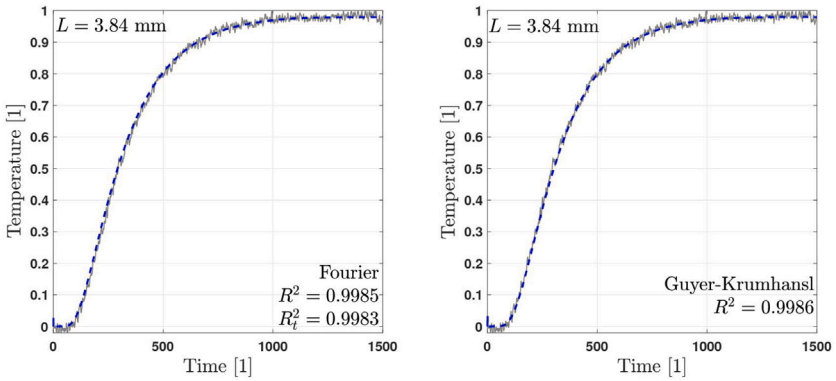

Fig. 10. The rear side temperature history for the basalt rock sample with $L = 3.84$ mm.

Table 3
Summarizing the fitted thermal parameters for the metal foam sample.

Metal foam sample	Findings in Ván et al. (2017) with Wolfram Math				Present algorithm			
	α_F 10^{-6} [m^2/s]	α_{GK} 10^{-6} [m^2/s]	τ_q [s]	κ^2 10^{-6} [m^2]	α_F 10^{-6} [m^2/s]	α_{GK} 10^{-6} [m^2/s]	τ_q [s]	κ^2 10^{-6} [m^2]
5.2 mm	3.04	2.373	0.402	2.89	3.91	3.01	0.304	2.203

5.2. Metal foam

Regarding the extent of the non-Fourier effect, the situation becomes remarkably different for the metal foam sample, presented first in Ván et al. (2017). The millimeter size inclusions can significantly influence the thermal behavior. The outcome is plotted in Fig. 11 together with the corresponding R^2 values. Table 3 helps to compare the fitted values found by Wolfram Mathematica to ours. Notwithstanding that the GK parameters are in correspondence, the most notable difference is in the thermal diffusivities, interestingly. The Fourier resonance parameter is found to be 2.395 with our procedure, compared to 3.04 in Ván et al. (2017). In both cases, the ratio of α_F and α_{GK} is found to be 1.28–1.29, which represents a deviation from Fourier's theory that is remarkable indeed. Interestingly, that largest sample provides the strongest over-diffusive effect. According to our present understanding, it is not only the sample size that matters, but also the mutual interaction of the parallel heat transfer channels. In this particular situation, the heat transfer by convection and radiation in the inclusions could be compared to the heat conduction in the bulk material. Since these heat transfer modes have significantly different time scales, they together manifest in such a non-Fourier effect.

6. Discussion and summary

We developed an algorithm to efficiently evaluate room temperature heat pulse experiments in which a non-Fourier effect could exist. This is called over-diffusive propagation and detunes the thermal diffusivity, even when the deviation is seemingly small or negligible for the rear side temperature history. The presented method is based on the analytical solution of the Guyer–Krumhansl equation, including temperature-dependent convection boundary condition, thus the heat transfer to the environment

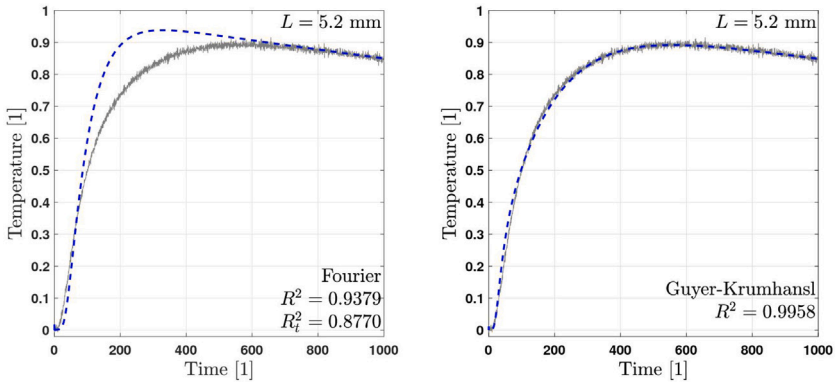

Fig. 11. The rear side temperature history for the metal foam sample with $L = 5.2$ mm.

can be immediately included in the analysis. The reevaluation of the preceding experiments showed an actual size dependence for all thermal parameters, especially for the GK coefficients τ_q and κ^2; however, we have to keep in mind that the samples are under their representative size. Furthermore, the results are in accordance with the outcome of the iterative 'brute force' fitting procedure of Wolfram Math, basically, but are yielded using far fewer computational resource.

We plan to improve this procedure by including the investigation of front side temperature history, too. When x_1 is obtained from the rear side, it could be easily used to describe the front side's thermal behavior. This is much more sensitive to the initial time evolution right after the excitation, therefore it could serve as a better candidate to achieve a more precise and robust estimation for the x_2 exponent. Also, having two temperature histories would be a remarkable step forward to confirm the occurrence of non-Fourier heat conduction in the experimental data.

We believe that this procedure lays the foundations for more practical engineering applications of non-Fourier models, especially for the best candidate among all of them, the Guyer–Krumhansl equation. It sheds new light on the classical and well-known flash experiments, and we provide the necessary tools to find additional thermal parameters to achieve a better description of heterogeneous materials. This is becoming increasingly important with the spreading of composites and foams and helps characterize 3D printed samples with various inclusions. The method presented in this paper facilitates the evaluation of heat pulse experiments, helping researchers identify the appearance of non-Fourier behavior more efficiently and obtain the coefficients as quickly as possible. By continuing the experiments, our goal is to find a relationship between the non-Fourier coefficients and the material structure. For instance, we aim to analyze multiple metal foam samples with different inclusion sizes, expecting to connect production parameters to the non-Fourier effects. Consequently, these results would allow the heterogeneous structure to be substituted with a homogeneous one in the modeling procedure, significantly decreasing the computational demand, e.g., of a finite element simulation. Moreover, such a relationship between the technological and material parameters would be extremely helpful in designing the material structure to exploit the over-diffusive phenomenon. In other words, one could predict the thermal transients without measuring each of the samples. Therefore, the development of a reliable evaluation procedure is a milestone on this journey.

From a computational point of view, such practical application of the Guyer–Krumhansl equation would require a proper numerical method. While the one-dimensional situations can be efficiently and reliably handled, the solution methods for three-dimensional problems are still not elaborated. The reason is that the usual finite element approach does not work (e.g., see examples for COMSOL Rieth et al., 2018) since the classical interpretation of boundary conditions is not valid anymore. Thus it is still under development. These research branches are converging to each other, pointing towards the practical embeddability of the Guyer–Krumhansl equation.

Acknowledgments

The authors thank Tamás Fülöp, Péter Ván, and Mátyás Szücs for the valuable discussions. We thank László Kovács (ROCKSTUDY Ltd. (Kőmérő Kft.), Hungary) and Tamás Bárczy (Admatis Kft., Hungary) for producing the rock and metal foam samples.

The research reported in this paper and carried out at BME has been supported by the grants National Research, Development and Innovation Office-NKFIH FK 134277 and by the NRDI Fund, Hungary (TKP2020 NC, Grant No. BME-NCS) based on the charter of bolster issued by the NRDI Office under the auspices of the Ministry for Innovation and Technology. This paper was supported by the János Bolyai Research Scholarship of the Hungarian Academy of Sciences, Hungary.

Appendix. Galerkin-type solution of heat equations

A.1. Notes on the boundary conditions

Since the non-Fourier models are not well-known in the general literature, there are only a few available analytical and numerical methods to solve such a spatially nonlocal equation like the Guyer–Krumhansl one. The nonlocal property is a cornerstone of these models since the usual boundary conditions do not work in the same way. That could be a problem when the outcome seemingly violates the maximum principle, see for instance Zhukovsky (2016b) in which the operational approach is applied (Zhukovsky, 2016a).

Another particular candidate originates from the spectral methods, it is called Galerkin method, where both the weight and the trial functions are the same. Fortunately, following Kovács (2018), we can surely apply sine and cosine trial functions in which terms the solution can be expressed. It is important to emphasize that we deal with a system of partial differential equations in our case. The physical (and mathematical) connection between the field variables restricts the family of trial functions. Namely, even in the simplest case of the Fourier heat equation,

$$\partial_t T + \partial_x q = 0, \quad q + \alpha \partial_x T = 0, \tag{20}$$

q and T are orthogonal to each other, and the trial functions must respect this property. Our choice is found by the method called separation of variables, but it resulted in a too complicated outcome due to the time-dependent boundary condition. In Kovács (2018), the heat pulse is modeled with a smooth $q_0(t) = 1 - \cos(2\pi t/t_p)$ function on the $0 < t \leq t_p$ interval. It is disadvantageous since the most interesting part falls beyond t_p, and the solution in $t_p < t$ must account for the state at the time instant t_p as an initial condition. Therefore, it results in cumbersome expressions for the coefficients.

We overcome this difficulty by introducing a different function to model the heat pulse, i.e., we use $q_0(t) = -(\exp(-C_1 t) - \exp(-C_2 t))/n$, where C_1 and C_2 are chosen to have a sufficiently small q_0 after t_p, hence the values are $C_1 = 1/0.075$ and $C_2 = 6$. The coefficient n normalizes q_0 to 1 from 0 to t_p, so it is $n = (C_1 - C_2)/(C_1 C_2)$ (with neglecting $\exp(-C_1)$ and $\exp(-C_2)$ terms, contributing negligibly to n). For larger time instants, the front side becomes adiabatic. Regarding the rear side boundary condition, we choose to take into account heat convection for both models.

(1) First, we restrict ourselves to the Fourier equation. According to our previous experiments (Both et al., 2016; Fülöp et al., 2018; Ván et al., 2017), the Fourier equation can be safely used where cooling effects become significant. This solution is used to estimate the heat transfer coefficient and the maximum temperature and to give a first approximation to the thermal diffusivity.
(2) In the second step, we repeat the calculation for the GK model with the same boundary conditions. We use the previously found Fourier parameters as the input to estimate the GK parameters and fine-tune the thermal diffusivity. The heat transfer coefficient and the temperature maximum can be kept the same.

A.2. Step 1: solving the Fourier equation

While there are several available solutions in the literature, we want to see how the Galerkin approach performs on this model using our set of dimensionless parameters and boundary conditions. This allows us to directly compare the two heat equation models. Let us recall the mathematical model for the sake of traceability. In the Fourier model, we have

$$\partial_t T + \partial_x q = 0, \quad q + \alpha \partial_x T = 0, \tag{21}$$

with

$$q_0(t) = -\frac{1}{n}\Big(\exp(-C_1 t) - \exp(-C_2 t)\Big), \quad n = \frac{C_1 - C_2}{C_1 C_2}, \quad q_1(t) = hT(x = 1, t), \tag{22}$$

in which all parameters are dimensionless, as presented in Section 2.2. The initial conditions are $q(x, t = 0) = 0$ and $T(x, t = 0) = 0$, the conducting medium is thermally relaxed. We emphasize that one does not need to separately specify boundary conditions for the temperature field T as well. Regarding the heat flux field q, we must separate the time-dependent part from the homogeneous one,

$$q(x, t) = w(x, t) + \tilde{q}(x, t), \quad w(x, t) = q_0(t) + x\left(q_1(t) - q_0(t)\right) \tag{23}$$

with $\tilde{q}$ being the homogeneous field and w inherits the entire time-dependent part from the boundary (and x runs from 0 to 1). The spectral decomposition of $\tilde{q}$ and T are

$$\tilde{q}(x, t) = \sum_{j=1}^{N} a_j(t)\phi_j(x), \quad T(x, t) = \sum_{j=1}^{N} b_j(t)\varphi_j(x), \tag{24}$$

with $\phi_j(x) = \sin(j\pi x)$ and $\varphi_j(x) = \cos(j\pi x)$. Revisiting the boundary conditions, q_0 is trivial, and q_1 becomes: $q_1(t) = hT(x = 1, t) = h\sum_{j=0}^{N} b_j(-1)^j$. Naturally, one has to represent also $w(x, t)$ in the space spanned by $\phi_j(x)$. After substituting these expressions into (21), multiplying them by the corresponding weight functions and integrating them in respect to x from 0 to 1, a system of ordinary

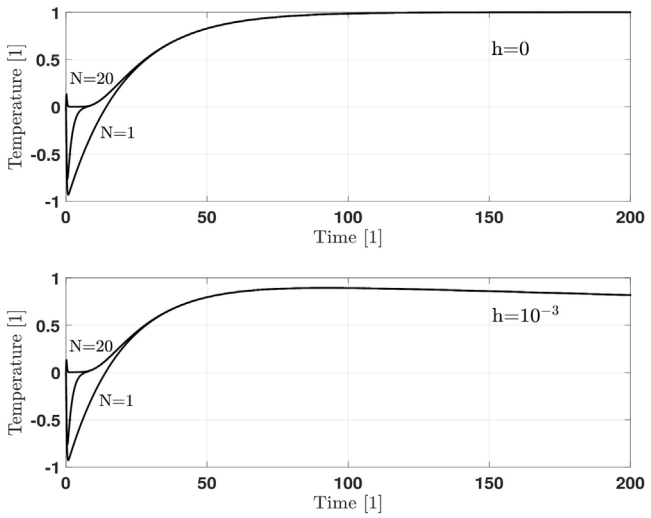

Fig. 12. Convergence analysis for the Fourier equation in two different cases on the rear side temperature history. The first shows the adiabatic limit, and the second presents the case when the heat transfer coefficient h is not zero. In both cases, we applied 1, 3 and 20 terms in the spectral decomposition (24), with $\alpha = 0.005$.

differential equations (ODE) is obtained. Here, we exploit the fact that the square of the trial functions $\phi(x)^2$ and $\varphi(x)^2$ are both integrable and after integration they are equal to $1/2$. Since the cos series has a non-zero part for $j = 0$, we handle it separately from the others corresponding to $j > 0$.

- For $j = 0$, we have

$$\dot{b}_0 + \partial_x w = 0, \rightarrow \dot{b}_0 = -hb_0 + q_0 \tag{25}$$

  with the upper dot denoting the time derivative, and $a_0 = 0$ identically.
- For $j > 0$, we obtained

$$\dot{b}_j + j\pi a_j = 0, \tag{26}$$

$$a_j = \alpha j\pi b_j + \frac{2}{j\pi}(hb_j - q_0), \tag{27}$$

  where the term $2/(j\pi)$ comes from the sin series expansion of w. We note that for $j > 0$, $\partial_x w$ does not contribute to the time evolution.

Such ODE can be solved easily both numerically and analytically for suitable q_0 functions. Fig. 12 shows the analytical solution programmed in Matlab in order to demonstrate the convergence to the right (physical) solution. In this respect, we refer to Rieth et al. (2018) in which a thorough analysis is presented on the analytical and numerical solution of heat equations beyond Fourier. Our interest is to utilize as few terms as possible of the infinite series, enough to be able to properly describe the rear side temperature history (i.e., the measured one) from a particular time instant. In other words, we want to simplify the complete solution as much as possible while keeping its physical meaning.

Starting with $j = 0$ case, we find that the terms in the particular solution with $\exp(-C_1 t)$ and $\exp(-C_2 t)$ extinct very quickly, thus we can safely neglect them while keeping the $\exp(-ht)$ as the leading term throughout the entire time interval we investigate. Briefly, $j = 0$ yields

$$b_0(t) = Y_0 \exp(-ht), \quad Y_0 = (C_1 - C_2)/\big(n(C_1 - h)(C_2 - h)\big). \tag{28}$$

Continuing with $j = 1$, we make the same simplifications and neglect the same exponential terms as previously after taking into account the initial condition, obtaining

$$b_1(t) = Y_1 \exp(-2ht)\exp(-\pi^2 t), \quad Y_1 = 2(C_1 - C_2)/\big(n(C_1 + x_F)(C_2 + x_F)\big), \quad x_F = -2h - \alpha\pi^2. \tag{29}$$

Based on the convergence analysis (Fig. 12), we suppose that these terms are eligible to properly describe the temperature history after $t > 30$ (which is equal to 0.3 s if $t_p = 0.01$ s). Finally, we can combine these solutions, thus $T(x = 1, t) = b_0 - b_1$ (the alternating sign originates in $\cos(j\pi)$).

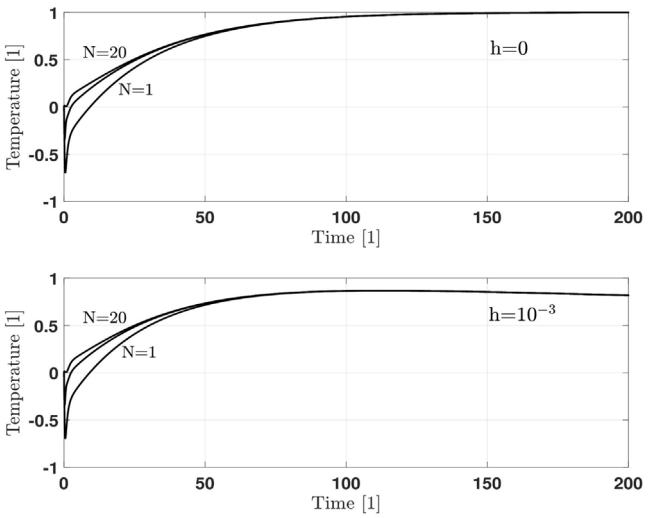

Fig. 13. Convergence analysis for the Guyer–Krumhansl equation in two different cases on the rear side temperature history. The upper figure shows the adiabatic limit, and the lower figure presents the case when the heat transfer coefficient h is not zero. In both cases, we applied 1, 3 and 20 terms in the spectral decomposition (24), with $\alpha = 0.005$, $\tau_q = 1$, and $\kappa^2 = 10\alpha\tau_q$.

A.3. Step 2: solving the Guyer–Krumhansl equation

Here, we repeat the calculations using the same set of trial and weight functions as for the GK model, that is, we solve

$$\partial_t T + \partial_x q = 0, \quad \tau_q \partial_t q + q + \alpha \partial_x T - \kappa^2 \partial_{xx} q = 0, \tag{30}$$

with

$$q_0(t) = -\Big(\exp(-C_1 t/t_p) - \exp(-C_2 t/t_p)\Big)/n, \quad q_1(t) = hT(x=1,t), \quad q(x,t=0) = 0, \quad T(x,t=0) = 0. \tag{31}$$

Analogously with the Fourier case, we obtain a set of ODE as follows.

- For $j = 0$, we have

$$\dot{b}_0 + \partial_x w = 0, \rightarrow \dot{b}_0 = -hb_0 + q_0, \tag{32}$$

  which is the same as previously due to $a_0 = 0$ identically.
- For $j > 0$, a_j changes

$$\dot{b}_j + j\pi a_j = 0, \tag{33}$$

$$\tau_q \dot{a}_j + \left(1 + \kappa^2 j^2 \pi^2\right) a_j = \alpha j \pi b_j + \frac{2}{j\pi}\left[(hb_j - q_0) + \tau_q(h\dot{b}_j - \dot{q}_0)\right]. \tag{34}$$

Consequently, the zeroth term, $b_0(t)$ remains the same with the particular solution being omitted,

$$b_0(t) = Y_0 \exp(-ht), \quad Y_0 = (C_1 - C_2)/\big(n(C_1 - h)(C_2 - h)\big). \tag{35}$$

However, for $b_1(t)$, the particular solution $P(t)$ becomes more important, its initial value influences the temperature history, i.e., $P_0 = P(t=0)$ and $DP_0 = \mathrm{d}_t P(t=0)$ appears in the coefficients Z_1 and Z_2, and the P_0 and DP_0 quantities are important in the evaluation method, too. Thus $b_1(t)$ reads

$$b_1(t) = Z_1 \exp(x_1 t) + Z_2 \exp(x_2 t) + P(t), \quad Z_1 = -\frac{DP_0 - P_0 x_2}{x_1 - x_2}, \quad Z_2 = -P_0 + \frac{DP_0 - P_0 x_2}{x_1 - x_2}. \tag{36}$$

The exponents x_1 and x_2 depend on the GK parameters τ_q and κ^2, and are obtained as the roots of the quadratic equation $x_j^2 + k_{1j}x + k_{2j} = 0$:

$$x_{1,2} = x_{j1,2} | j = 1, \quad x_{j1,2} = \frac{1}{2}\left(-k_{1j} \pm \sqrt{k_{1j}^2 - 4k_{2j}}\right), \quad k_{1j} = \frac{1 + \kappa^2 j^2 \pi^2}{\tau_q} + 2h, \quad k_{2j} = \frac{\alpha j^2 \pi^2}{\tau_q} + \frac{2h}{\tau_q}. \tag{37}$$

Furthermore, the particular solution reads as

$$P_j(t) = M_{j1} \exp(-C_1 t) + M_{j2} \exp(-C_2 t), \quad M_{j1} = \left(\frac{2C_1}{n} - \frac{2}{n\tau_q}\right) / \left[k_{2j} - k_{1j}C_1 + C_1^2\right],$$

$$M_{j2} = \left(-\frac{2C_2}{n} + \frac{2}{n\tau_q} \right) / \left[k_{2j} - k_{1j} C_2 + C_2^2 \right]. \tag{38}$$

Hence $P_0 = M_1 + M_2$ and $DP_0 = -M_1 C_1 - M_2 C_2$ appears in $b_1(t)$ with $j = 1$, too. After obtaining Z_1 and Z_2, $P(t)$ can be neglected since it becomes negligibly small at $t > t_p$. Finally, we formulate the rear side temperature history using $b_0(t)$ and $b_1(t)$ as

$$T(x = 1, t) = b_0 - b_1 = Y_0 \exp(-ht) - Z_1 \exp(x_1 t) - Z_2 \exp(x_2 t), \tag{39}$$

for which Fig. 13 shows the convergence property and that 'one-term solution' provides sufficient accuracy with $t > 40$.

References

Both, S., Czél, B., Fülöp, T., Gróf, Gy., Gyenis, Á., Kovács, R., et al. (2016). Deviation from the Fourier law in room-temperature heat pulse experiments. *Journal of Non-Equilibrium Thermodynamics*, *41*(1), 41–48.

Cimmelli, V. A. (2009). Different thermodynamic theories and different heat conduction laws. *Journal of Non-Equilibrium Thermodynamics*, *34*(4), 299–333.

Dreyer, W., & Struchtrup, H. (1993). Heat pulse experiments revisited. *Continuum Mechanics and Thermodynamics*, *5*, 3–50.

Fabrizio, M., & Franchi, F. (2014). Delayed thermal models: stability and thermodynamics. *Journal of Thermal Stresses*, *37*(2), 160–173.

Fabrizio, M., Lazzari, B., & Tibullo, V. (2017). Stability and thermodynamic restrictions for a dual-phase-lag thermal model. *Journal of Non-Equilibrium Thermodynamics*, Published Online:2017/01/10.

Fülöp, T., Kovács, R., Lovas, Á., Rieth, Á., Fodor, T., Szücs, M., et al. (2018). Emergence of non-Fourier hierarchies. *Entropy*, *20*(11), 832, arXiv:1808.06858.

Fülöp, T., Kovács, R., & Ván, P. (2015). Thermodynamic hierarchies of evolution equations. *Proceedings of the Estonian Academy of Sciences*, *64*(3), 389–395.

Guyer, R. A., & Krumhansl, J. A. (1966a). Solution of the linearized phonon Boltzmann equation. *Physical Review*, *148*(2), 766–778.

Guyer, R. A., & Krumhansl, J. A. (1966b). Thermal conductivity, second sound, and phonon hydrodynamic phenomena in nonmetallic crystals. *Physical Review*, *148*, 778–788.

James, H. M. (1980). Some extensions of the flash method of measuring thermal diffusivity. *Journal of Applied Physics*, *51*(9), 4666–4672.

Joseph, D. D., & Preziosi, L. (1989). Heat waves. *Reviews of Modern Physics*, *61*(1), 41.

Józsa, V., & Kovács, R. (2020). *Solving problems in thermal engineering: a toolbox for engineers*. Springer.

Kovács, R. (2018). Analytic solution of guyer-krumhansl equation for laser flash experiments. *International Journal of Heat and Mass Transfer*, *127*, 631–636.

Kovács, R., & Ván, P. (2015). Generalized heat conduction in heat pulse experiments. *International Journal of Heat and Mass Transfer*, *83*, 613–620.

Landau, L. (1947). On the theory of superfluidity of helium II. *Journal of Physics*, *11*(1), 91–92.

Mitra, K., Kumar, S., Vedevarz, A., & Moallemi, M. K. (1995). Experimental evidence of hyperbolic heat conduction in processed meat. *ournal of Heat Transfer*, *117*(3), 568–573.

Müller, I., & Ruggeri, T. (1998). *Rational extended thermodynamics*. Springer.

Nyíri, B. (1991). On the entropy current. *Journal of Non-Equilibrium Thermodynamics*, *16*(2), 179–186.

Parker, W. J., Jenkins, R. J., Butler, C. P., & Abbott, G. L. (1961). Flash method of determining thermal diffusivity, heat capacity, and thermal conductivity. *Journal of Applied Physics*, *32*(9), 1679–1684.

Rieth, Á., Kovács, R., & Fülöp, T. (2018). Implicit numerical schemes for generalized heat conduction equations. *International Journal of Heat and Mass Transfer*, *126*, 1177–1182.

Rukolaine, S. A. (2014). Unphysical effects of the dual-phase-lag model of heat conduction. *International Journal of Heat and Mass Transfer*, *78*, 58–63.

Rukolaine, S. A. (2017). Unphysical effects of the dual-phase-lag model of heat conduction: higher-order approximations. *International Journal of Thermal Sciences*, *113*, 83–88.

Sobolev, S. L. (1994). Heat conduction equation for systems with an inhomogeneous internal structure. *Journal of Engineering Physics and Thermophysics*, *66*(4), 436–440.

Sobolev, S. L. (1997). Local non-equilibrium transport models. *Physics-Uspekhi*, *40*(10), 1043–1053.

Sobolev, S. L. (2014). Nonlocal diffusion models: Application to rapid solidification of binary mixtures. *International Journal of Heat and Mass Transfer*, *71*, 295–302.

Sobolev, S. L. (2016). Nonlocal two-temperature model: Application to heat transport in metals irradiated by ultrashort laser pulses. *International Journal of Heat and Mass Transfer*, *94*, 138–144.

Tisza, L. (1938). Transport phenomena in helium II. *Nature*, *141*, 913.

Tzou, D. Y. (2014). Longitudinal and transverse phonon transport in dielectric crystals. *ournal of Heat Transfer*, *136*(4), Article 042401.

Ván, P. (2001). Weakly nonlocal irreversible thermodynamics – the guyer-krumhansl and the cahn-hilliard equations. *Physics Letters. A*, *290*(1–2), 88–92.

Ván, P. (2016). Theories and heat pulse experiments of non-Fourier heat conduction. *Communications in Applied and Industrial Mathematics*, *7*(2), 150–166.

Ván, P., Berezovski, A., Fülöp, T., Gróf, Gy., Kovács, R., Lovas, Á., et al. (2017). Guyer-krumhansl-type heat conduction at room temperature. *EPL*, *118*(5), 50005, arXiv:1704.00341v1.

Ván, P., & Fülöp, T. (2012). Universality in heat conduction theory – weakly nonlocal thermodynamics. *Annalen Der Physik (Berlin)*, *524*(8), 470–478.

Zhukovsky, K. V. (2016a). Exact solution of guyer–krumhansl type heat equation by operational method. *International Journal of Heat and Mass Transfer*, *96*, 132–144.

Zhukovsky, K. (2016b). Violation of the maximum principle and negative solutions for pulse propagation in guyer–krumhansl model. *International Journal of Heat and Mass Transfer*, *98*, 523–529.